Thermoelastic Instability for the Transient Contact Problem of Two Sliding Half-Planes

A. Azarkhin[1]
Product Engineering Division,
Aluminum Company of America,
Alcoa Center, PA 15069

J. R. Barber
Department of Mechanical Engineering and
Applied Mechanics,
University of Michigan,
Ann Arbor, MI 48109

We study the time dependent problem of a nonconducting half-plane sliding on the surface of a conductor with heat generation at the interface due to friction. The conducting half-plane is slightly rounded to give a Hertzian initial pressure distribution. Relationships are established for temperature and thermoelastic displacements due to a heat input of cosine type through the surface, and then these are used to obtain the solution in the form of a double Fourier integral. Numerical results show that, if the ratio of the initial size of the area of contact to that in the steady state is less than some critical value, the area of contact and the pressure distribution change smoothly toward the steady state solution. Otherwise the area of contact goes through bifurcation. The bifurcation accelerates the process. Numerical results are compared with previous approximate solutions.

1 Introduction

It is now well known that the pressure development at the partially contacting surfaces of two sliding bodies can be unstable in the process involving frictional heating (Barber, 1967; Barber, 1969; Burton et al., 1973a; Burton and Nerlikar, 1975; Dow and Burton, 1972). In the absence of wear, the process tends to a known steady state (Barber, 1976; Burton et al., 1973b; Burton and Nerlikar, 1974). Interest in the transient process leading to this steady state is motivated by its application to brake design and operating conditions (Parker and Marshall, 1948; Barber et al., 1985). In papers by Barber (1980) and Barber et al. (1985), the thermoelastic displacements were approximated by a quadratic surface which resulted in considerable simplification of the governing equations. A more accurate solution of the problem was given by Azarkhin and Barber (1985), where the algorithm presented was based on utilization of transient Green's functions given by Barber and Martin-Moran (1982) for temperature and thermoelastic displacements, giving a representation of the problem in terms of the unknown pressure on the surface. The implementation of the algorithm indicated that for sufficiently large ratio of the initial width of the contact area to that in the steady state, bifurcation would occur. However, it proved impossible to treat this case because of consideration of computational time and accuracy, which also prevented the nonbifurcating case being pursued as far as the steady state.

The object of the present work is to overcome these difficulties and extend the range of time so as to follow the process from the beginning to the steady state. This is achieved by a volume rather than the surface representation of the variables. We first study relationships for a wavy perturbation of the temperature of the form $\cos(mx)\cos(ny)\exp(-\sigma t)$ and then show how this can be used to present the temperature and the stress state in the form of a double Fourier integral with m and n changing continuously. Finally, we present some numerical results and compare them with previous approximate solutions.

2 The Model

We assume that:

1) The contact area is stationary with respect to one solid,
2) The other solid is a rigid nonconductor,
3) There is no coupling between tangential and normal tractions,
4) The conducting body is slightly rounded to give initial Hertzian pressure distribution.
5) The uncoupled theory of thermoelasticity is used.

The implications of these idealizations are discussed in more detail by the authors earlier (Azarkhin and Barber, 1985). In particular, we note that assumption (3) does not mean that the tangential tractions on the surface are neglected. Indeed the work done against these tractions is the source of the heat flux. However, the elastic displacements normal to the surface, caused by the tangential tractions, are much smaller than those produced by the normal tractions and the coupling effect is negligible. This simplification is frequently made in the solution of contact problems with frictional sliding. Kuznetsov (1978) examines the magnitude of the error which can be anticipated and refers to other studies of the subject. We also note that the approximation becomes exact if constant β introduced by Dundurs (1969) is zero.

[1] Formerly at the Department of Mechanical Engineering and Applied Mechanics, University of Michigan, Ann Arbor, MI 48109.

Contributed by the Applied Mechanics Division for presentation at the Winter Annual Meeting, Anaheim, CA, December 7–12, 1986, of the American Society of Mechanical Engineers.

Discussion on this paper should be addressed to the Editorial Department, ASME, United Engineering Center, 345 East 47th Street, New York, N.Y. 10017, and will be accepted until two months after final publication of the paper itself in the JOURNAL OF APPLIED MECHANICS. Manuscript received by ASME Applied Mechanics Division, March 4, 1985; final revision January 31, 1986. Paper No. 86-WA/APM-29.

3 Governing Equations and Boundary Conditions

The temperature is governed by the equation

$$\frac{\partial^2 T}{\partial x^2}+\frac{\partial^2 T}{\partial y^2}=\frac{1}{k}\frac{\partial T}{\partial t} \tag{1}$$

with the boundary condition

$$K\frac{\partial T}{\partial y}=-\mu p V \qquad y=0,\ x\geq 0 \tag{2}$$

where K is conductivity of material, diffusivity $k=K/\rho\, c$ and μ, p, V are, respectively, the coefficient of friction, contact pressure, and sliding speed. Equation (2) states that the heat generated due to friction flows locally into the conducting body.

The thermoelastic displacements are governed by the equations:

$$(1-\nu)\frac{\partial^2 u}{\partial x^2}+\frac{(1-2\nu)}{2}\frac{\partial^2 u}{\partial y^2}+\frac{1}{2}\frac{\partial^2 v}{\partial x\partial y}=\alpha(1+\nu)\frac{\partial T}{\partial x} \tag{3}$$

$$(1-\nu)\frac{\partial^2 v}{\partial y^2}+\frac{(1-2\nu)}{2}\frac{\partial^2 v}{\partial x^2}+\frac{1}{2}\frac{\partial^2 u}{\partial x\partial y}=\alpha(1+\nu)\frac{\partial T}{\partial y} \tag{4}$$

(see Timoshenko and Goodier, 1970, p. 465), where ν is Poisson's ratio, α is linear expansion coefficient, and u, v are the displacement components in x and y coordinate directions, respectively. The origin is placed in the middle of the area of contact and the y axis directed into the body.

The boundary conditions can be written

$$p(x,t)=-\sigma_{yy}(x,0,t)\geq 0 \qquad x\leq A(t) \tag{5}$$

$$v(x,0,t)\geq C-\frac{x^2}{2R} \qquad x\geq A(t) \tag{6}$$

$$v(x,0,t)=C-\frac{x^2}{2R} \qquad x\leq A(t) \tag{7}$$

$$\sigma_{yy}(x,0,t)=0 \qquad x>A(t) \tag{8}$$

$$2\int_0^{A(t)} p(x)dx=P(t) \tag{9}$$

$$\sigma_{xy}(x,0,t)=\mu p(x,t) \qquad x\leq A(t)$$
$$=0 \qquad x>A(t)$$

In these equations, $A(t)$ is the half-width of the area of contact, $P(t)$ is the prescribed force pressing the bodies together, the term $x^2/2R$ describes the roundedness of the body, C is an arbitrary rigid body displacement, and

$$\sigma_{yy}=\frac{E(1-\nu)}{(1+\nu)(1-2\nu)}\frac{\partial v}{\partial y}+\frac{\nu E}{(1+\nu)(1-2\nu)}\frac{\partial u}{\partial x}-\frac{\alpha E T}{1-2\nu} \tag{11}$$

$$\sigma_{xy}=\frac{E}{2(1+\nu)}\left(\frac{\partial u}{\partial y}+\frac{\partial v}{\partial x}\right) \tag{12}$$

In view of assumption (3) (see section 2 above), the tangential tractions on $y=0$ have negligible effect on $v(x, 0, t)$, except of course through their effect on the frictional heat flux which is implicit in equation (2). It follows that the solution of equations (2) and (5)–(9) for $p(x, t)$ is uninfluenced by equation (10) and hence $p(x, t)$ is always symmetrical about $x=0$ and the equations can be written for the range $x\geq 0$. The equations as stated imply that the area of contact is simply connected, but generalization to the case of several contact areas is straightforward.

These relationships define the solution to the problem, including the area of contact, which is unknown a priori.

4 Dimensionless Formulation

For constant load P and speed V, the number of parameters can be reduced by introducing the dimensionless variables

$$x^*=x/A_o \tag{13} \qquad A^*(t)=A(t)/A_o \tag{14}$$

$$T^*=3\pi k\rho cT/(4\mu PV) \tag{15} \qquad p^*=pA_o/P \tag{16}$$

$$t^*=kt/A_o^2 \tag{17}.$$

where A_o is the half-width of the area of contact in the steady state.

It is shown (Azarkhin and Barber, 1985) that the most interesting quantities—the dimensionless pressure p^*, the half-width of the contact area $A^*(t^*)$, and the temperature T^*—depend on a single dimensionless parameter

$$A^*(0)=A(0)/\left(\frac{3\pi(1-\nu)k\rho c}{4\alpha\mu VE}\right) \tag{18}$$

which is the ratio of the initial contact area to the steady state value.

It is therefore possible to absorb all physical parameters into one coefficient, velocity, say, and there is no loss of generality in taking $\nu=0$, $A(0)=1$, $\mu=1$, $E=1$, $k=1$, $\rho=1$, $c=1$, $E=1$. This results in considerable simplification of all the equations. One can especially appreciate omitting Poisson's ratio. For example, equation (11) becomes simply

$$\sigma_{yy}=\frac{\partial v}{\partial y}-T. \tag{19}$$

It also allows us to write expressions for thermoelastic displacements in terms of m and n explicitly (see equations (27) and (28) below). In the following discussion we assume that this replacement has already been performed.

5 Preview of the Algorithm

The transient problem is discretized by dividing the process into small increments of time. The contact pressure, and hence heat input are then presented as piecewise constant functions with respect to time and updated at the end of each time step. For any particular time step the heat input is expanded into the Fourier integral

$$\frac{\partial T}{\partial n}=-\int_o^\infty A_m\cos(mx)dx \tag{20}$$

where

$$A_m=-\frac{2}{\pi}\int_o^{A(t)}\frac{\partial T}{\partial n}\cos(mx)dx \tag{21}$$

The displacements of the half-plane are sought as a sum of thermoelastic displacements corresponding to a traction free surface, u_{th} and v_{th}, and elastic displacements u_e, v_e caused by the superposed contact pressure.

In view of equation (20), the thermoelastic displacements and temperature can be expressed as a series of terms of the form $f_m(y, t)\cos(mx)$ (see equations (24), (27)–(31) below) where $f_m(y, t)$ are unknown functions which are determined from the boundary conditions during the time step and the initial temperature distribution at the beginning of the time step. When computations for a current time step are completed, we move the origin to the end of the time step and the functions are updated using a recurrent relation (37).

The superimposed contact pressure for each time step is found from the integral equation, following from equation (7) and expressed in terms of the Green's function:

$$v_{th}+\int_{-A(t)}^{A(t)} p(z)G(x,z)dz$$

$$\equiv v_{th}+\frac{2}{\pi}\int_{-A(t)}^{A(t)} p(z)\log|x-z|dz=C-\frac{x^2}{2R} \tag{22}$$

The solution to this equation is subject to constraints (5), (6), and (9). This defines the area of contact which is not known a priori and has to be found by iteration. A convergent iterative procedure for the search for the area of contact and its numerical implementation are described in sections 8 and 9.

6 Results for a Sinusoidal Temperature Distribution

Suppose that the heat input through the surface has the form

$$\frac{\partial T}{\partial n} = -A_m \cos(mx) \tag{23}$$

where A_m is a constant. The temperature in the body is then given by

$$T = \frac{A_m}{m} T_m(y,t)\cos(mx) \equiv \frac{A_m}{m}\Big\{\exp(-my) + \int_o^\infty C_m(n)\cos(ny)\exp[-(m^2+n^2)t]dn\Big\}\cos(mx) \tag{24}$$

which is also a definition for $T_m(y, t)$. The first term on the right hand side of equation (24) represents the steady state solution. Functions $C_m(n)$ in the second, decaying term are defined by the initial conditions

$$C_m(n) = \frac{2}{\pi}\int_o^\infty [T_m(y,0) - \exp(-my)]\cos(ny)dy \tag{25}$$

The integrand in equation (25) is the difference between the initial and steady state temperature distributions. In particular, for the initial step of the process $T_m(y, 0) = 0$ and

$$C_m(n) \equiv C_m^o(n) = -\frac{2}{\pi}\frac{m}{(m^2+n^2)} \tag{26}$$

We present displacements as a sum of thermoelastic displacements, u_{th} and v_{th}, corresponding to traction free boundary condition, and elastic displacements caused by the superimposed pressure $p(x, t)$ which brings the two bodies into contact. The thermoelastic displacements can be written in the form

$$u_{th} = \frac{A_m}{m^2} u_m(y,t)\sin(mx) \equiv \frac{A_m}{m^2}\Big\{D_m(t)[\exp(-my) - my\exp(-my)] + \int_o^\infty B_m(n,t)\cos(ny)dn + \exp(-my)\Big\}\sin(mx) \tag{27}$$

$$v_{th} = \frac{A_m}{m^2} v_m(y,t)\cos(mx) \equiv \frac{A_m}{m^2}\Big\{(D_m(t)-1)\exp(-my) - D_m(t)(my+3)\exp(-my) + m\int_o^\infty F_m(n,t)\sin(ny)dn\Big\}\cos(mx) \tag{28}$$

where these equations constitute definitions of u_m and v_m. These expressions satisfy the boundary condition (10) identically when substituted into equation (12) and also satisfy equations (3) and (4) if

$$F_m(n,t) = \frac{nC_m(n)}{(m^2+n^2)}\exp[-(m^2+n^2)t] \tag{29}$$

$$B_m(n,t) = \frac{mC_m(n)}{(m^2+n^2)}\exp[-(m^2+n^2)t] \tag{30}$$

The functions D_m are obtained from the traction free boundary condition ($\sigma_{yy} = 0$ on $y = 0$) using equation (11). We find

$$D_m(t) = m^2\int_o^\infty \frac{C_m(n)\exp[-(m^2+n^2)t]dn}{(m^2+n^2)} \tag{31}$$

7 Fourier Integral Representation

The results of the previous section can be used as the basis of a Fourier integral representation of the thermoelastic field in a body subjected to a heat input of the more general type

$$\frac{\partial T}{\partial y} = f(x) \tag{32}$$

We write

$$T(x,y,t) = \int_o^\infty \frac{A_m}{m} T_m(y,t)\cos(mx)dm \tag{33}$$

$$u_{th}(x,y,t) = \int_o^\infty \frac{A_m}{m^2} u_m(y,t)\sin(mx)dm \tag{34}$$

$$v_{th}(x,y,t) = \int_o^\infty \frac{A_m}{m^2} v_m(y,t)\cos(mx)dm \tag{35}$$

in which case equation (32) is satisfied if A_m is defined by equation (21).

8 Contact Pressure: Algorithm and Numerical Implementation

We start with initial temperature zero and the Hertzian pressure distribution

$$p(x) = \frac{2P}{\pi A(0)}\left\{1 - \left[\frac{x}{A(0)}\right]^2\right\}^{1/2} \tag{36}$$

The corresponding heat input (equation (2)) is considered to be constant for a small period of time Δt. The heat input is expanded into the Fourier integral representation according to equations (20) and (21) where $\partial T/\partial n = \mu p V$. This step defines the function A_m. Since $C_m(n)$, $F_m(n, t)$ and D_m are known from equations (26), (29), and (31), the thermoelastic displacements v_{th} at time Δt can be found from equation (28). This makes it possible to update the thermal bulge at the end of the time interval. The corresponding contact pressure can then be found as the solution to the integral equation (22). For the numerical implementation the pressure is represented as a polygon with nodes distributed uniformly over the area of contact. The unknowns are the pressures at these nodes and the constant C in equation (7). They can be found from the system of algebraic equations which is obtained from equation (7) written for each interior node. One more equation comes from a numerical analog of equation (6). The area of contact is not known a priori but can be found by iteration. If the area of contact was not guessed correctly, tensile pressure will occur at some nodes and (or) overlapping of the bodies at others. We then release the nodes of the first type and introduce contact for the nodes of the second type, and repeat the procedure. The convergence of this algorithm will be discussed in section 9 below.

It is worth noting that at first we used a variational formulation of the problem with a penalty approach to approximate the contact inequalities. However, the direct iteration on the inequality constraints discussed above was found to be considerably more efficient numerically.

Suppose that the area of contact has been found at the end of the time step, and both the pressure and the functions A_m have been updated. We can now move the origin for time to the end of the time step Δt, and update the coefficients $C_m(n)$ from the condition that the temperature at the end of the previous time step is equal to that at the start of the next step. This gives the recurrence relation:

$$C_m^+(n) = C_m^o(n)\left[\frac{A_m^-}{A_m^+} - 1\right] + C_m^-(n)\frac{A_m^-}{A_m^+}\exp[-(m^2+n^2)\Delta t] \tag{37}$$

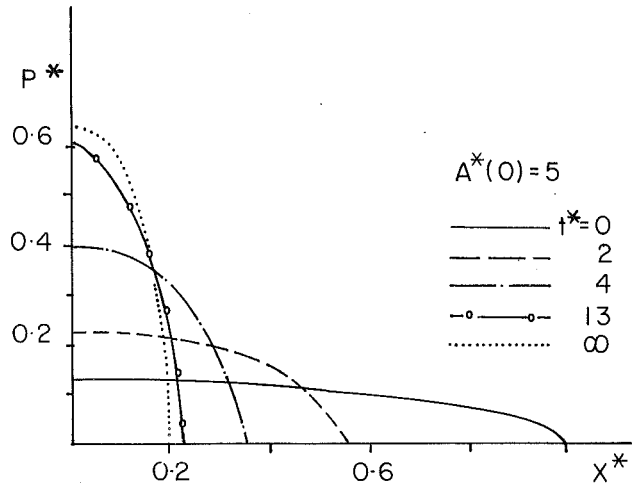

Fig. 1 Devlopment of the pressure distribution for $A^*(0) = 5$

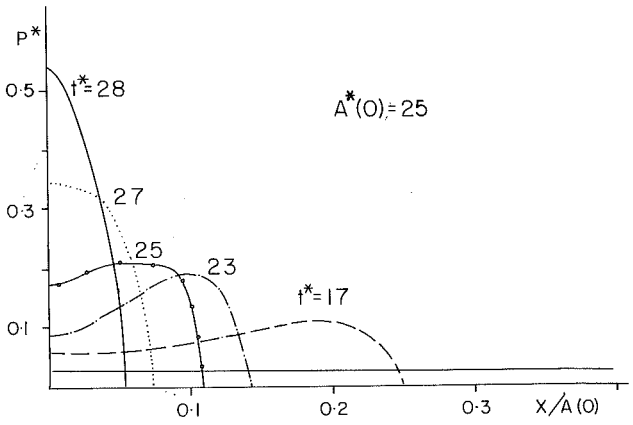

Fig. 3 Development of the pressure distribution for $A^*(0) = 25$

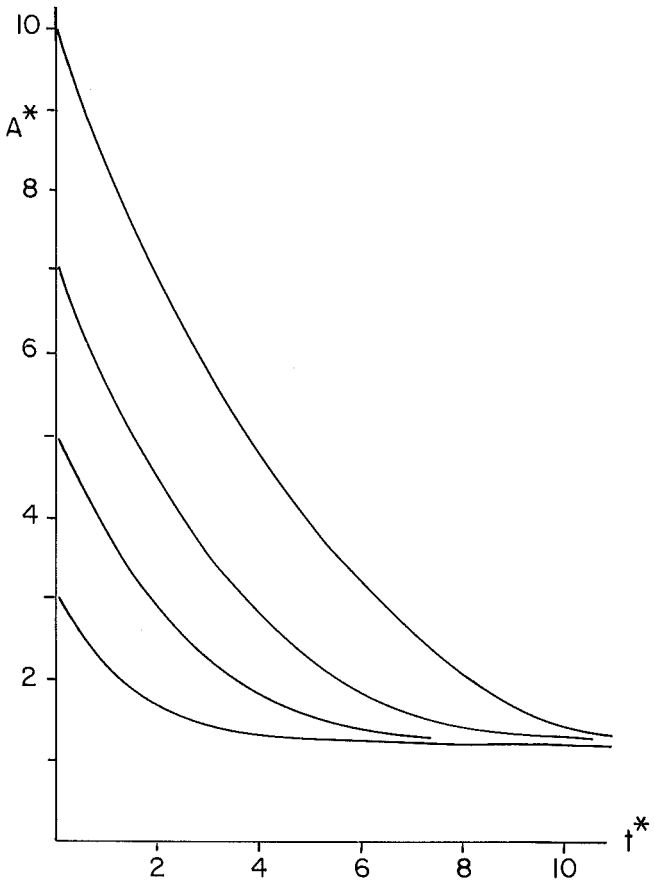

Fig. 2 Reduction of the area of contact with time for $A^*(0) \leq 10$

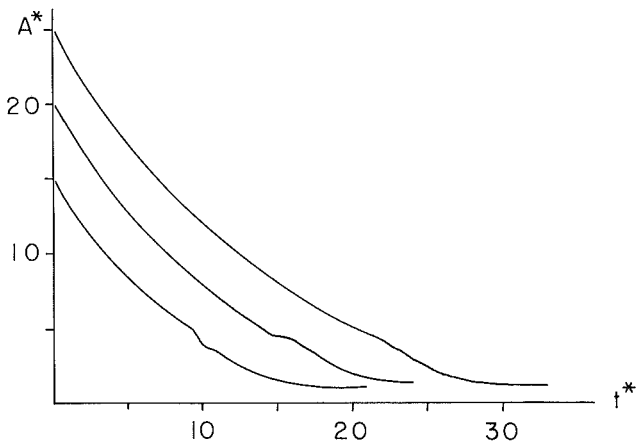

Fig. 4 Reduction of the area of contact with time for $A^*(0) = 15, 20, 25$

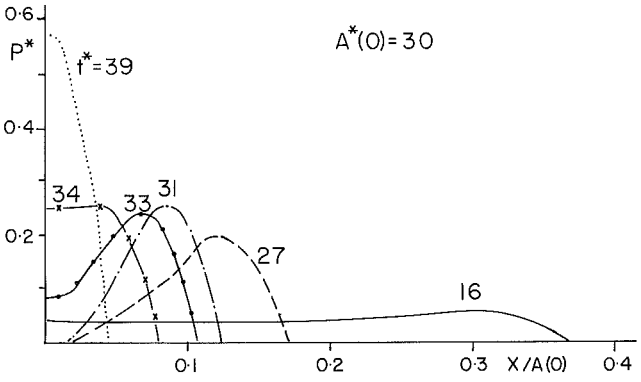

Fig. 5 Development of the pressure distribution for $A^*(0) = 30$

where superscripts + or − relate, respectively, to the previous and consecutive time steps, and $C^o m(n)$ are defined by equation (26).

Expressions (33)–(35) contain infinite limits of integration, but an integral in a finite range can be obtained by the change of variable

$$g = \left(\frac{m}{m+n}\right) \tag{38}$$

We note that for the first time step

$$C_m(n)dn = C_m^o(n)dn = \frac{2}{\pi}\frac{mdn}{(m^2+n^2)}$$

$$= \frac{2}{\pi}\frac{dg}{[g^2+(1-g)^2]} \tag{39}$$

and the dependence on m vanishes. This attractive feature is not preserved for the consecutive time steps, but the transformation (equation (38)) still gives good numerical accuracy for the numerical integration procedure.

9 Search for the Area of Contact: Convergence of the Algorithm

It is conceivable that the iterative algorithm for determining the extent of the contact area should not converge—for example, the release of nodes which require tensile tractions for contact could cause overlapping to occur at one or more nodes at the next iteration. However, we note that the release of the tensile area is equivalent to an application of compressive stresses at the released area, self-equilibrated somewhere else

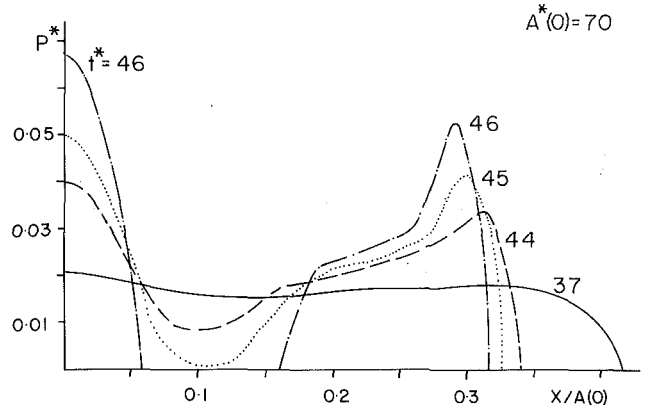

Fig. 6(a) Earlier stage of process

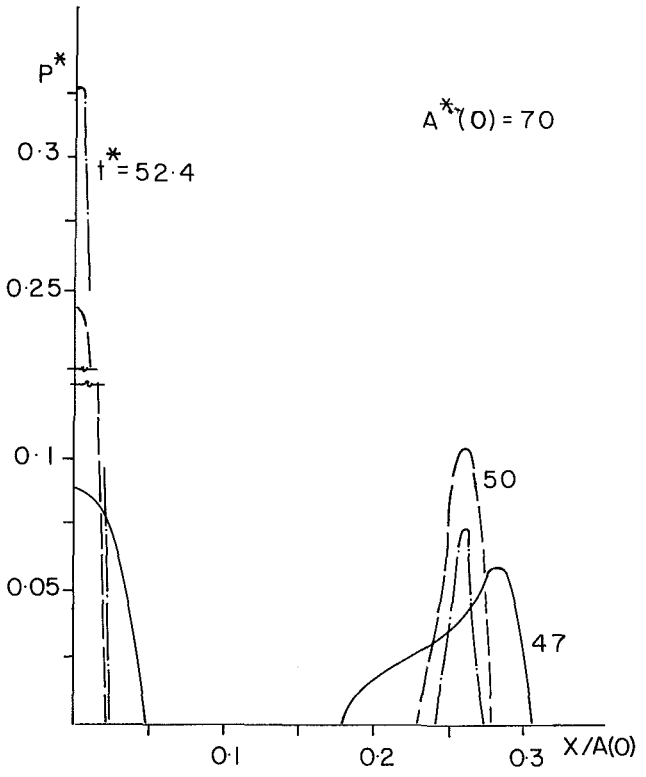

Fig. 6(b) After bifurcation

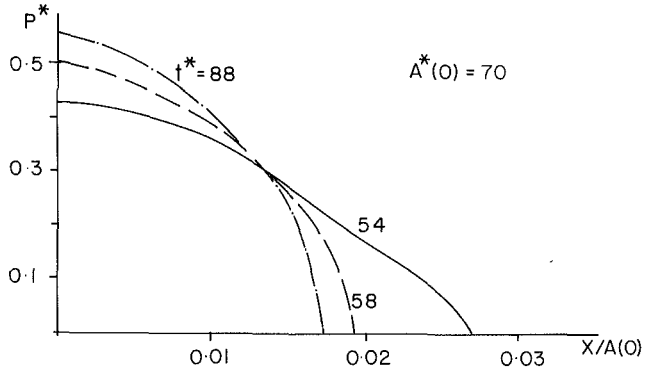

Fig. 6(c) Midpoint takes over the whole load

Fig. 6 Development of the pressure distribution for $A^*(0) = 70$

in the remaining portion of the contacting area. It can be shown by integration by parts of the integral in equation (22) that this does not change the rigid body displacement C in equation (7), and with this constraint, it is proved (Barber, 1974) that the additional displacements of the surface caused by the self-equilibrated load are nonnegative. It follows that the iterative procedure converges monontonically on the solution which satisfies the inequalities (equations (5) and (9)).

This conclusion was supported by the numerical results. With a finite number of nodes, the iterative process terminates after a finite number of steps. Approximately three iterations were required on average, and in the worst case—where the contact area was multiply connected—only five iterations were required.

10 Numerical Results

Numerical solutions were obtained for values of $A^*(0)$ in the range 3 to 100. The improved algorithm permitted us to track the process from the start to an advanced stage which was close to the steady state.

For $A^*(0) \leq 10$, both the pressure and the area of contact changed smoothly with the progress of time, tending to the steady state solutions. An example of the pressure development for $A^*(0) = 5$ is shown in Fig. 1. Figure 2 shows how the contact area shrinks with time for various initial values.

For $A^*(0) = 15$, 20, and 25 some waviness was observed in the pressure distribution in the intermediate stage. However, this tendency was not strong enough to cause bifurcation of the contact area. In effect, the reduction in contact area is too rapid in these cases for the waviness to develop into bifurcation, as can be seen from the contact pressure distribution in Fig. 3 for $A^*(0) = 25$. The variation of contact area with time for these cases is shown in Fig. 4. Notice that each of the curves shows a slight irregularity near $A^* = 5$, which is associated in each case with a transition from a trough to a peak at $x = 0$. In Fig. 5 for $A^*(0) = 30$, the pressure follows the same pattern at first, but this time waviness is sufficient to cause bifurcation, and the mid-point loses contact. Then the contact regions (one is the mirror image of the other) move to the middle until they merge; still later maximum pressure is established at the midpoint, and the pressure converges to the steady state.

The larger the ratio $A^*(0)$, the more contact regions are developed during the bifurcation phase. For example, three regions are developed for $A^*(0) = 70$ and five for $A^*(0) = 100$. The development of the pressure for these two ratios is shown in Figs. 6 and 7. The pattern of pressure variation differs from that for $A^*(0) = 30$. The maximum is established at the midpoint at the start and after bifurcation the maximum pressure for each region grows with time. However, the rate of growth is different at the different regions and eventually the process is reversed for all regions except one which takes over the whole load.

Variation of contact area with time is shown in Fig. 8. Broken lines represent the bifurcation phase of the process for which A^* is interpreted as the sum of contact zone dimensions. We can see that bifurcation accelerates the process of convergence to the steady state.

The temperature variation at the midpoint for $A^*(0)$ in the range from 3 to 10 is given in Fig. 9. All the curves eventually converge, as might be anticipated, since the size of the steady state area of contact is approximately the same ($A_o = 1$). In Fig. 10, development of the temperature for larger values of $A^*(0)$ is given. The flat piece of the curve for $A^*(0) = 30$ in the interval $24 \leq t^* \leq 28$ is due to temporary separation at the midpoint. The curves for $A^*(0) = 70$ and 100 are close in the interval $47 \leq t^* \leq 50$. A possible explanation is that the bifurcation for both cases is over at that time, and areas of contact are almost the same (see Fig. 8). Later, however, the two curves diverge slightly.

11 Comparison with Previous Solutions

We now compare the present results with the previous numerical solution (Azarkhin and Barber, 1985) and with the approximate solution based on a Hertzian distribution (Barber, 1980). Since neither of these solutions was able to treat the bifurcation phase of the process, we concentrate attention on the comparison of results for $A^*(0) \leq 25$.

The present results agree with those of Azarkhin and Barber (1985) during the earlier stage of the process, but later the two solutions diverge. Typical results are shown in Fig. 11 for $A^*(0) = 10$, where the solid line represents the present results and the broken line the earlier results. The source of this discrepancy was identified in the earlier paper. The contribution to the thermal distortion of the heat input which occurred at time t during an interval Δt was computed as an integral with limits t and $t - \Delta t$. When t is large, the results are obtained as a small difference between two large numbers and become progressivly inaccurate. For the purpose of the present comparison, an improved version of the previous solution was developed in which this difficulty was overcome by replacing the corresponding terms with the solutions for a point source. This replacement (small circles in Fig. 11) shows good agreement with the present results. In general, the present technique is more efficient at an advanced stage of the

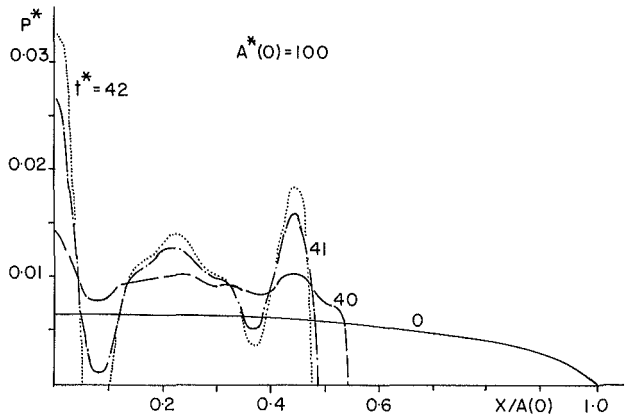

Fig. 7(a) Earlier stage of the process; first bifurcation

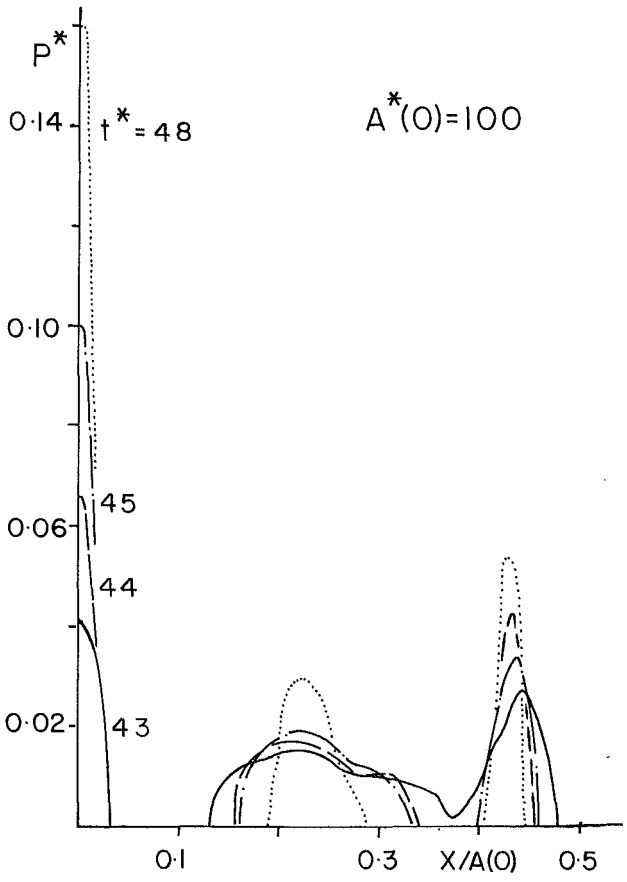

Fig. 7(b) Two more regions of contact develop

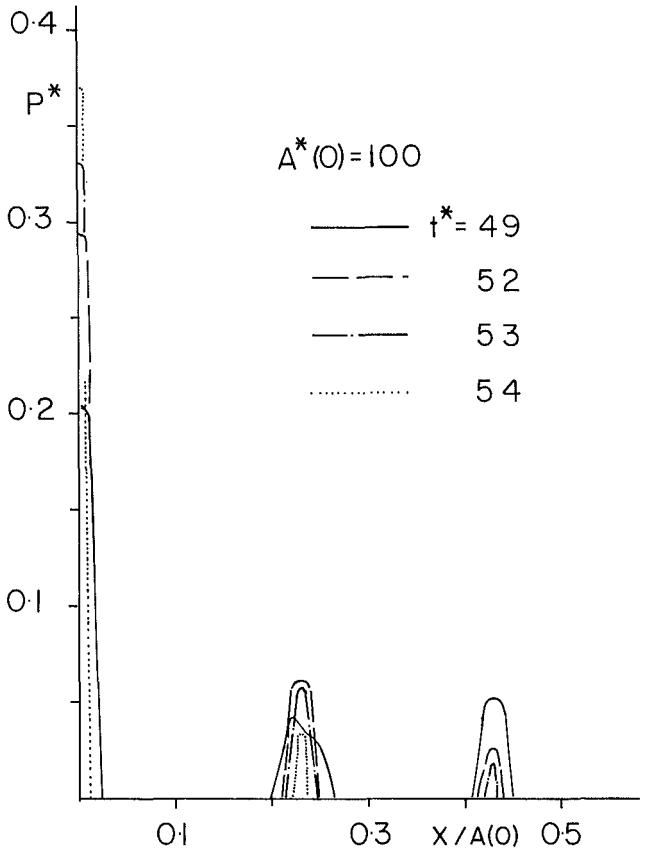

Fig. 7(c) Decrease of the pressure at all the regions except the midpoint

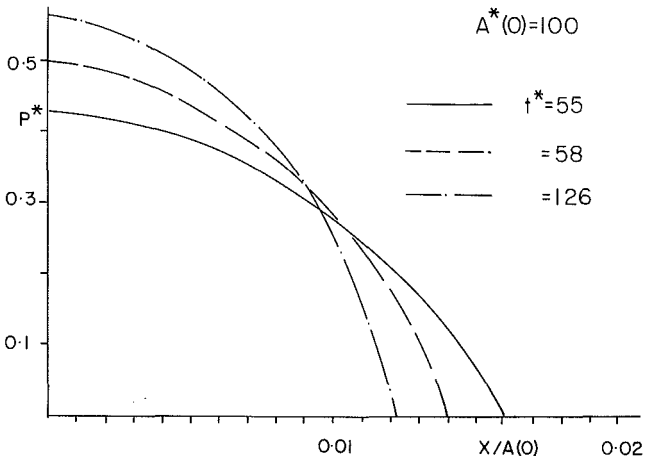

Fig. 7(d) The midpoint takes over the whole pressure

Fig. 7 Development of the pressure distribution for $A^*(0) = 100$

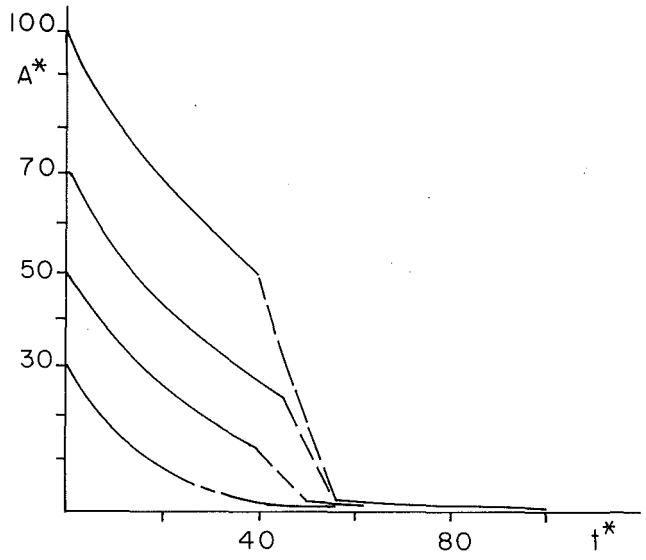

Fig. 8 Reduction of the area of contact with time for $A^*(0) = 30$, 50, 70, and 100

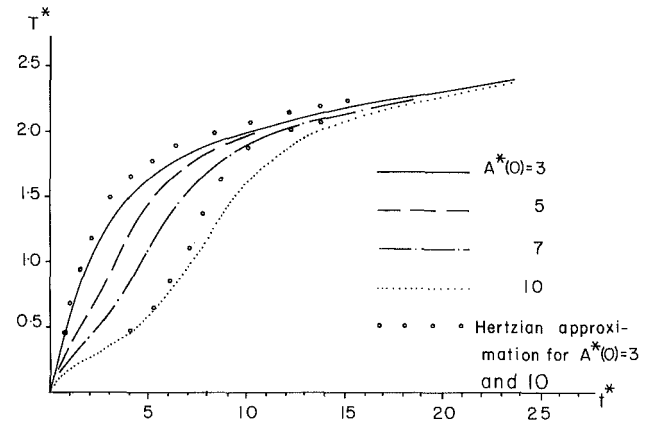

Fig. 9 Dimensionless temperature at the midpoint for $A^*(0) = 3$, 5, 7, 10

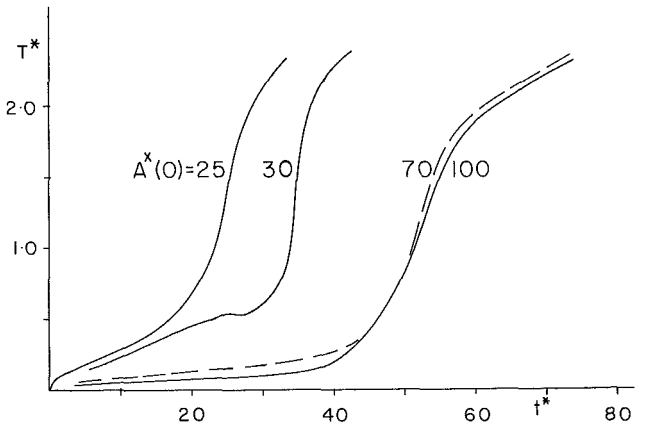

Fig. 10 Dimensionless temperature at the midpoint for $A^*(0) = 25$, 30, 70, 100

process, but its particular advantage is of course that it allows us to follow the process through bifurcation for $A^*(0) \geq 30$. Notice however, that the algorithm developed before is more efficient for the earlier stages of the process. Figure 11 also shows results for the simplified model, based on the Hertzian approximation, for $A^*(0) = 3$, 10. This method gives an order of magnitude estimate of the reduction of contact area with time.

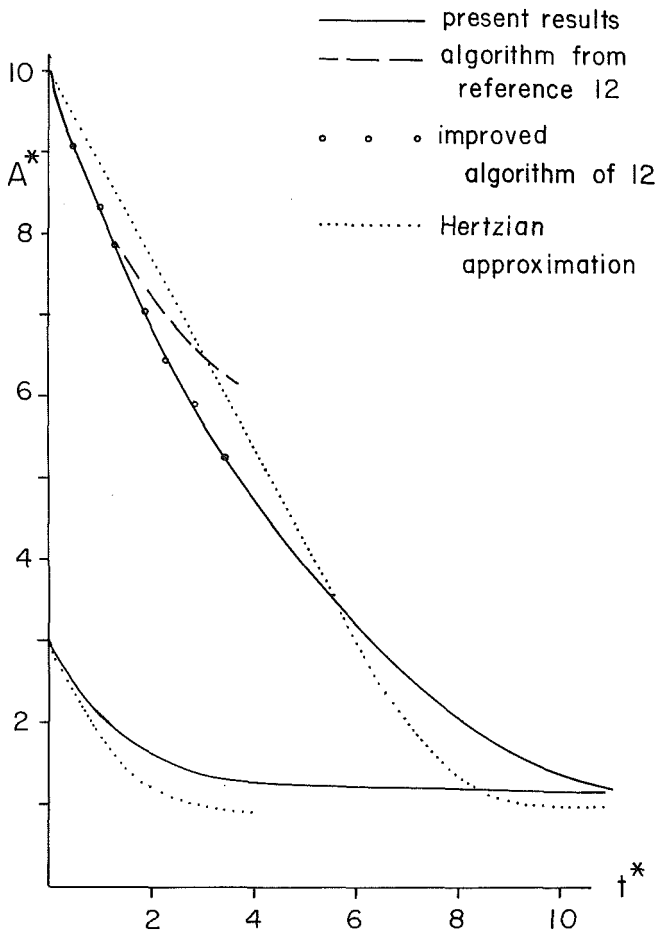

Fig. 11 Comparison with the simplified model. Reduction of the area of contact for $A^*(0) = 3$, 10

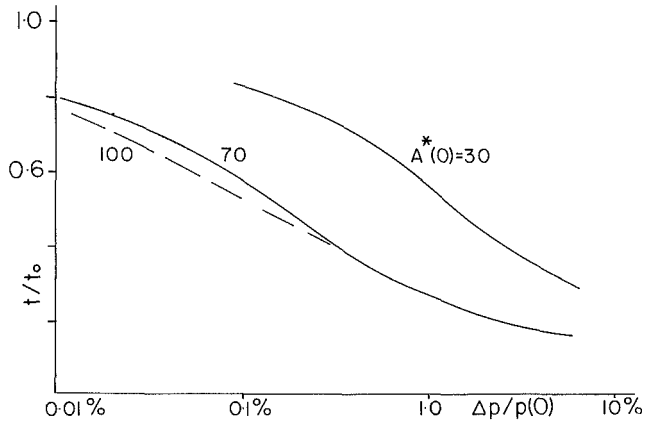

Fig. 12 Influence of a wavy perturbation of the surface on the time at which bifurcation occurs

The temperature at the midpoint predicted by the Hertzian approximation are compared with the present accurate results in Fig. 9. For small values of t^* the approximate theory gives good results, but at larger t^* the temperature is overestimated, as we might anticipate, since the approximate solution converges to a steady state contact area which is 15 percent smaller than the known exact solution given by Barber (1976).

However, the approximate solution is sufficiently accurate to justify its use—with the consequent large saving in computing time—when the initial contact area is not large enough to cause bifurcation to occur.

12 Sensitivity Analysis

Since the transient process of pressure distribution and area of contact development is unstable for sufficiently large ratios $A^*(0)$, it is reasonable to expect that small changes introduced by the data or numerical implementation might produce considerable changes in the results. It is interesting to know for which ratios $A^*(0)$ this is the case. To answer this question, we superposed some additional waviness on the surface of the body

$$\delta = \delta_o \cos(mx)$$

where m was chosen to correspond to the wave of maximum growth rate (see Dow and Burton, 1972; and Azarkhin and Barber, 1985). The results are given in Fig. 12, where the relative time of bifurcation t/t_o is plotted against the relative amplitude of the initial pressure perturbation $\Delta p/p(0) \times 100$ percent. In this figure, t is the bifurcation time and t_o is the bifurcation time for the unperturbed surface. Inspection of the curves shows that the required accuracy of implementation is high and unlikely to be reached. Therefore, the pressure development shown in Figs. 6 and 7 can be viewed as a pattern rather than taken literally. In general, we note that the transient development of the instability is very sensitive to the existence of an initial waviness of appropriate wavelength.

In a practical sliding system waviness will be developed due to nonuniform wear during previous periods of sliding. Thus, sliding surfaces which have previously experienced thermoelastic instability behavior will be liable to develop it more rapidly on subsequent occasions.

Acknowledgments

J. R. Barber gratefully acknowledges support from the National Science Foundation under grant number MSM-8419324.

References

Azarkhin, A., and Barber, J. R., 1985, "Transient Thermoelastic Contact Problem of Two Sliding Half-Planes," *Wear*, Vol. 102, pp. 1–13.

Barber, J. R., 1967, "The Influence of Thermal Expansion on the Friction and Wear Process," *Wear*, Vol. 10, pp. 155–159.

Barber, J. R., 1969, "Thermaelastic Instabilities in the Sliding of Conforming Solids," *Proc. Roy. Soc.*, A312, pp. 381–394.

Barber, J. R., 1974, "Determining the Contact Area in Elastic—Indentation Problems," *J. Strain Analysis*, Vol. 9(4), pp. 230–232.

Barber, J. R., 1976, "Some Thermoelastic Contact Problems Involving Frictional Heating," *Q. J. Mech. Appl. Math.*, Vol. 29, pp. 1–13.

Barber, J. R., 1980, "The Transient Thermoelastic Contact of a Sphere Sliding on a Plane," *Wear*, Vol. 59, pp. 1–9.

Barber, J. R., Beamond, T. W., Waring, J. R., and Pritchard, C., 1985, "Implications of Thermoelastic Instability for the Design of Brakes," ASME *J. Tribology*, Vol. 107, pp. 206–210.

Barber, J. R., and Martin-Moran, C. J., 1982, "Green's Functions for Transient Thermoelastic Contact Problems for the Half-Plane," *Wear*, Vol. 79, pp. 11–19.

Burton, R. A., Nerlikar, V., and Kilaparti, S. R., 1973a, "Thermoelastic Instability in a Seal-Like Configuration," *Wear*, Vol. 24, pp. 177–188.

Burton, R. A., Kilparti, S. R., and Nerlikar, V., 1973b, "A Limiting Stationary Configuration with Partially Contacting Surfaces," *Wear*, Vol. 24, pp. 199–206.

Burton, R. A., and Nerlikar, V., 1974, "Effect of Initial Surface Curvature on Frictionally Excited Thermoelastic Phenomena," *Wear*, Vol. 27, pp. 195–207.

Burton, R. A., and Nerlikar, V., 1975, "Large Disturbance Solution for Initially Flat Frictionally Heated Thermoelastically Deformed Surfaces," ASME *J. Lubr. Tech.*., Vol. 97, pp. 546–551.

Dow, Th.A., and Burton, R. A., 1972, "Thermoelastic Instability of Sliding Contact in the Absence of Wear," *Wear*, Vol. 19, pp. 315–328.

Dundurs, J., 1969, "Discussion," ASME JOURNAL OF APPLIED MECHANICS, Vol. 36, pp. 650–652.

Kuznetsov, E. A., 1978, "Superposition Principle in the Solution of Contact Problems with Allowance for Friction," *Soviet Applied Mechanics*, Vol. 14, pp. 494–498.

Parker, R. C., and Marshall, P. R., 1948, "The Measurement of the Temperature of Sliding Surfaces, with Particular References to Railway Blocks," *Proc. Inst. Mech. Eng.*, Vol. 158, pp. 207–229.

Timoshenko, S. P., and Goodier, J. N., 1970, *Theory of Elasticity*, McGraw-Hill, N.Y.